
Article:
Dai, R. and Long, H. orcid.org/0000-0003-1673-1193 (2025) Formation mechanism of subsurface white etching area and white etching crack of failed bearings in wind turbine gearbox. Wear, 582-583. 206335. ISSN: 0043-1648

https://doi.org/10.1016/j.wear.2025.206335

Wear 582–583 (2025) 206335 https://doi.org/10.1016/j.wear.2025.206335

Formation Mechanism of Subsurface White Etching Area and White Etching Crack of Failed Bearings in Wind Turbine Gearbox

R. Dai and H. Long*

School of Mechanical, Aerospace and Civil Engineering, the University of Sheffield, United Kingdom

*Corresponding author, email address: h.long@sheffield.ac.uk

Address: School of Mechanical, Aerospace and Civil Engineering, the University of Sheffield, Sir Frederick Mappin Building, S1 3JD, Sheffield, United Kingdom

Abstract

Bearings of some wind turbine (WT) gearboxes experienced premature failures due to bearing steel microstructural damage under rolling contact fatigue (RCF). However, the formation mechanism of the microstructural damage and its progression to the final bearing failure is still being debated. In this study, subsurface damage sustained in two bearing raceways of a failed gearbox from a field-operated WT is investigated. The study provides evidence of damage initiation and progression from non-metallic inclusions in the subsurface by using actually failed WT bearings as a case study. Damage characterisation has found various microstructural damage in the raceway subsurface including non-metallic inclusions, butterfly wing cracks, White Etching Areas (WEAs), and White Etching Crack (WECs). Complex interactions between cyclic rolling contact loading with inclusions and cracks are observed. Their roles in the formation of butterfly wing cracks, WEAs and WECs in the raceway subsurface are evaluated. It has been found that the butterfly wing cracks initiated at damaged inclusions is the original cause of the microstructural damage. The propagation of butterfly wing cracks and WEAs to form subsurface crack networks, with WEAs to create WECs, under RCF loading they have accelerated surface flaking and spalling of the raceways, leading to the final failure of the bearings. The formation mechanism of the subsurface initiated WEAs and WECs is evaluated and a damage progression hypothesis leading to the final bearing failure is proposed, including six stages of the microstructural damage development.

Key words: bearing; rolling contact fatigue; microstructural damage; white etching area; white etching crack.

1. Introduction

Wind Turbines (WT) gearbox bearings can fail prematurely, some with considerably shorter life than their designed service life of 20~25 years. Existing studies suggested that this was caused by the subsurface Rolling Contact Fatigue (RCF) initiated by non-metallic inclusions in the steel material of bearings [1]. During the steel manufacturing, aluminium element could be added to the steel, which worked as the deoxidiser to improve the steel toughness by controlling the growth of the austenite grain boundary [2]. Aluminium was easy to be oxidised, especially when the temperature was relatively high, and the oxidised Al_2O_3 inclusions formed were hard and brittle [3]. Therefore, it

could lead to localised cracks or voids in the subsurface of bearing raceways during the bearing manufacturing process and loading during operational service [4]. Another non-metallic element, sulphur, is also commonly found in the subsurface of the bearing raceways. Sulphur improves the machineability and it can be found in the form of manganese sulphide (MnS) or iron sulphide (FeS) in the subsurface of the bearing raceways. Non-metallic inclusions were found to affect the steel quality [5] and reduced both fatigue endurance limit and fracture toughness of the bearing steel [6, 7]. Due to the stress concentration caused by these inclusions, the cracking in the subsurface of the bearing raceways could occur easily and propagate rapidly in the bearing steel containing sufficiently high numbers of aluminium and sulphide inclusions [8].

The existence of the subsurface inclusions influences the homogeneity of the steel material in the subsurface of the bearing raceways and they can accelerate the crack nucleation and propagation processes. A number of mechanisms of the inclusion initiated damage have been proposed. Firstly, it could be caused by the differences of the thermal expansion coefficient between the steel matrix and an inclusion during the heat treatment processes of the steel. When the thermal expansion coefficient of the inclusion is greater or less than that of the steel matrix, it could lead to the boundary separation or cavitation between the inclusion and steel matrix. Secondly, the differences in the elastic modulus, yielding strength, and plastic deformation between the inclusion and steel material could also lead to the subsurface damage. As reported in [9], the maximum contact pressure generated on the planetary bearing surface of the WT gearbox could reach 3.2 GPa, which caused large deformations of both the steel matrix and inclusion materials. As a result, the differences of the corresponding deformation of the inclusion and the steel matrix could result in the formation of cavities and the separation of the original perfectly bonded boundary between the inclusion and steel matrix. In addition, the investigation in [9] also observed that the internal cracking of an inclusion could lead to the generation of subsurface cracks. According to their microscope observations, it was found that the internal crack of the inclusions had propagated from the inclusion to the steel matrix [9]. In their follow-up study based on the twin-disc experiment [10], it was found that the internal cracks of the inclusions were more likely to occur when the testing specimens were subjected to high contact pressures and impact loading conditions.

The propagated cracks in the subsurface of the bearing raceways are found to be accompanied by a hardened and phase transformed steel matrix, known as the White Etching Area (WEA). Existing studies had shown that the presence of WEAs on the propagated subsurface cracks further led to a reduced bearing life [8, 9]. Evidence obtained in [11] and [12] showed that WEAs had the body-centred (BCC) carbide-free ferrite with an ultrafine nano-recrystallised structure. The dense grain structure of a metallic material can impede dislocations between grain boundaries, thereby increasing the hardness of the material. Therefore, the ultra-fine ferrite in the WEA region differed from the ordinary ferrite material; its fine grain structure caused the hardness of this region to exceed that of the martensite matrix [13]. Another study in [14] reported that different WEAs also had different hardnesses. Such differences might be related to the grain sizes of different WEAs; with the reduction of the grain sizes, the hardness of WEAs was increased. Many WEAs have been found

within long crack networks in the subsurface of failed bearing raceways due to RCF loading. The long crack networks surrounded or decorated by WEAs are commonly referred as White Etching Cracks (WECs). A few studies suggested that WECs were initiated by butterfly wing damage from inclusions, voids or other subsurface defects and propagated under RCF loading cycles [15, 16, 17, 18]. However, some studies did not observe any inclusions within the WECs, indicating that the formation of WECs under RCF could be independent of the inclusions in the subsurface [19, 20].

According to the observations of the microstructures from the damaged bearings reported in [21, 22, 23, 24], it was generally agreed that the white etching damage was always accompanied by the occurrence of RCF cracks. Although the sequence between the white etching structure and RCF cracks was still being debated, the findings from [8] suggested that WEAs could lead to the premature failure of the bearings within 5% to 20% of their designed service life. A combined effect of WEAs under RCF was observed to accelerate the failure of WT gearbox bearings [25]. However, the sequence of formation between the WEA damage and RCF cracks has not been clearly established in published studies. Investigations in [15, 26, 27] believed that the formation of subsurface RCF cracks could be the root cause of the WEA damage. In addition, there could be the formation of Dark Etching Areas (DEAs) before the RCF crack formation, which indicated that the stiffness of the material was reduced, as evidenced in [28]. An investigation in [29] suggested that WEAs could be formed before the RCF cracks; and it was because of the hardening of the material caused by WEAs that RCF cracks could initiate from the specific region of the WEAs. Some other studies had shown that the WEA formation depended on a variety of factors rather than just RCF cracks. For example, the effect of electrical current was believed to have a significant effect on the formation of WEAs, reported in [30, 31]. Furthermore, the existence of hydrogen within the subsurface could also lead to an accelerated initiation of WEAs, as reported in [32, 33, 34, 35].

It is clear that the WEA and WEC related microstructural damage of WT gearbox bearings is extremely complex and still under intense investigations. A clear understanding has not been established regarding the formation mechanism of WEAs and WECs under RCF loading in WT operation condition, which leads to the premature failure of some WT gearbox bearings. In this study, the subsurface microstructural damage of two failed WT gearbox bearing raceways is evaluated to identify various forms of subsurface microstructural damages, including inclusions, butterfly wing cracks, WEAs, WECs, surface white structural flaking and resulting secondary crack networks. The root causes and interactions of these microstructural damages are investigated which leads to new insights into the formation mechanism of WEAs and WECs, and a new damage progression hypothesis that eventually leads to the premature failure of the WT gearbox bearings.

2. Methods and Materials

2.1 Sample preparation for microstructure observation

In this study, the subsurface areas of two failed planetary bearings from the gearbox of a 2MW WT operated in a wind farm in Europe are investigated to characterise microstructural damage. Both bearing raceways are made of 100Cr6 steel. The chemical composition of the 100Cr6 steel is provided

in Appendix Table A.1. Fig. 1 shows the failed inner raceway of the upwind and downwind planetary bearings of the gearbox, respectively. The damaged surface with spalling area and indenting area can be seen clearly on the raceway surface. Each raceway has a concentrated damage area, caused by the fixed loading zone of the raceway, as illustrated in Fig. 1a. For the planetary stage of the WT gearbox, the upwind bearing is located on the rotor side of the gearbox, facing the wind, and the downwind bearing is positioned next to the upwind bearing but on the higher speed side of the gearbox. The upwind bearing raceway in Fig. 1b shows severe spalling damage than that of the downwind bearing raceway in Fig. 1c. This is due to the different levels of the radial load acting on each bearing. It is known that in the WT gearbox the upwind planetary bearing normally undertook 40% to 60% more loads than the downwind bearing [36, 37]. Accordingly, the upwind bearing raceway shows a relatively larger area of surface spalling.

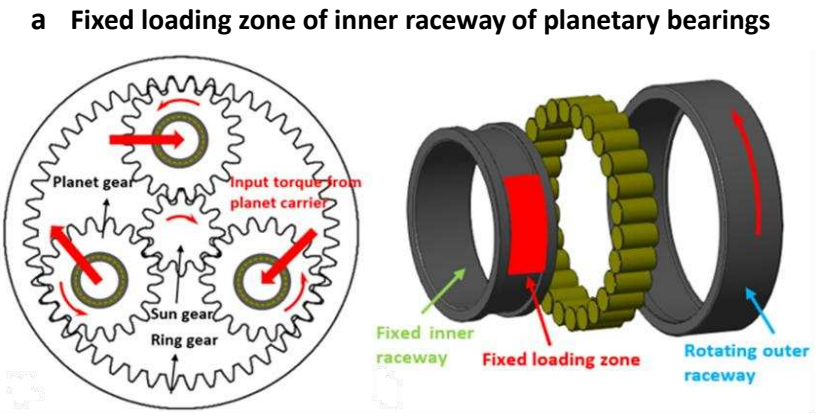

Fig. 1 Inner raceways of planetary bearings: (a) Illustration of fixed loading zone; (b) damaged raceway of upwind bearing; (c) damaged raceway of downwind bearing

To investigate three-dimensional structures of inclusions and crack networks in the raceway subsurface, the spalled surface area of both the upwind and downwind bearing raceways is sectioned along the axial and circumferential direction of the bearings respectively. After cutting, these small samples are mounted onto conductive Bakelite mounts. Processes of grinding and polishing are performed to ensure the smooth surface of the samples for observation. To observe the possible white etching damage around inclusions and subsurface cracks, etching process of the sample observing surfaces is performed by using the 2% Nital solution. In this study, both optical microscopy and scanning electron microscopy (SEM) are used to investigate subsurface damages of the raceways.

2.2 FE modelling of stress variation at inclusion under rolling contact fatigue

To investigate the stress distribution in the raceway subsurface under rolling contact condition, finite element (FE) models using Abaqus FE software platform are developed, representing a roller moves over the contact surface of the raceway, as shown in Fig.2a. Sizes of inclusions observed in the subsurface of the raceways are extremely small (in the range of 5~10 µm) thus the computational cost of using 3D meshing is excessively high, a 2D model has to be employed for effective FE simulations. Furthermore, for roller bearings, the raceways can be considered as plane strain condition in the axial direction of the bearings under RCF loading; therefore the 2D FE model in plane strain is adopted in this study. A simplified rectangle raceway section is created with width of $8b$ and depth of $4b$, where b is the half contact width between the roller and raceway; this is based on the consideration that the dimensions of 8b x 4b of the FE model are sufficient to avoid the effect of model boundary conditions on stress conditions around the inclusion. Furthermore, the majority of the subsurface damages from inclusions is observed within 1 mm to the contact surface of the raceway. Considering the rated condition of the 2MW WT investigated in this study, the maximum contact pressure and half contact width between the roller and raceway are calculated as 2.069 GPa and 0.531 mm respectively by using the Hertz contact theory. The detailed calculation of the Hertz contact parameters of the planetary bearings for the 2MW WT can be found in [38]. In the FE modelling, the distributed contact pressure moves from the left-hand side to the right-hand side of the rectangular raceway section with a constant speed of $6b$/s, i.e. within 1s. To simulate the rolling contact loading, two user subroutines in Abaqus are developed; the first one is a DLOAD subroutine, which defines the magnitude and movement of the Hertz contact pressure distribution on the raceway surface. The second subroutine is a UTRACLOAD, which defines the traction pressure distribution on the raceway surface due to the effect of friction.

To investigate the effect of an inclusion on stress variation in the raceway subsurface, a MnS inclusion is embedded in the subsurface area at 0.398 mm below the contact surface of the raceway. This is because the maximum shear stress occurs at this subsurface depth (0.398 mm) under the maximum contact pressure of 2.069 MPa thus the FE model investigates the most severe condition of an inclusion for damage development. The inclusion has an aspect ratio of two, with length in major and minor axes as 10 µm and 5 µm respectively. The selection of the inclusion sizes is based on the average value of the sizes of inclusions observed in actual samples of the failed bearing raceways. Three conditions of the inclusion are considered, perfectly bonded with the steel matrix of the

raceway (undamaged), separated from the steel matrix with two gaps at the inclusion tips, and internally cracked but perfectly bonded with the steel matrix. The conditions of the inclusion and the choice of an MnS inclusion are determined from the microstructural damage analysis, which will be presented in Section 3.

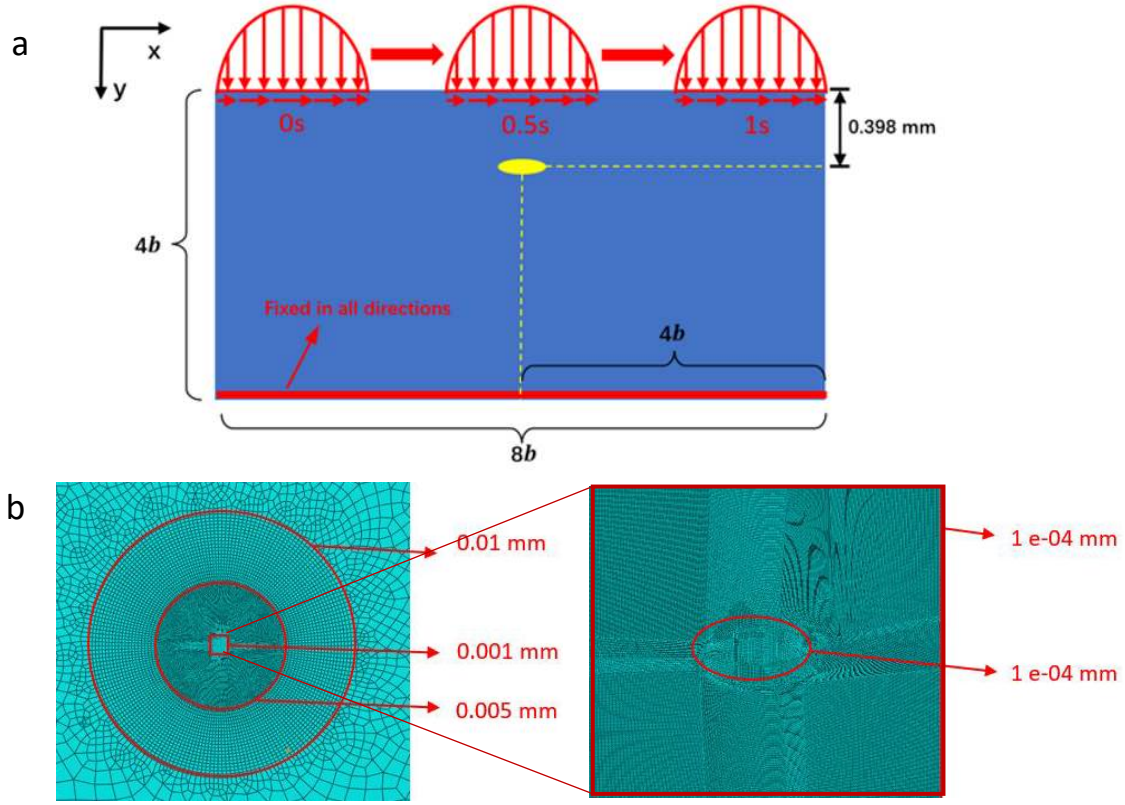

Fig.2 Finite element modelling of raceway rolling contact with subsurface inclusion: (a) global raceway model; (b) the global model mesh and partitions (on the left) and the sub-model mesh containing the inclusion (on the right, in square dimensions in 30 µm x 30 µm). The numerical values are the element sizes of the highlighted partitions of the FE meshes.

To obtain an accurate stress distribution around the inclusion, a sub-model of the global raceway rolling contact model for each inclusion condition is created; the sub-model has a square geometry in dimensions of 30 µm x 30 µm containing the inclusion with the size of 10 µm x 5 µm, the chosen mesh size for the sub-model is 1e-04 mm, as shown in Fig. 2b. The global model is divided into different partitions to facilitate the mesh divisions with extremely small element sizes, the representative mesh size for each partition of the FE mesh is provided individually in Fig. 2b. Regarding the boundary conditions, for the rectangular raceway section of the global model, displacements in the x-direction are constrained on both sides of the model and the bottom surface of the model is also fixed. The traction coefficient on the rolling contact surface is defined as 0.01. For the global raceway model, the total number of elements is 93,000 and the number of nodes is 94,000. In the sub-model, the number of elements is 95,000 and the number of nodes is 96,000. The raceway material is 100Cr6 steel with Young's Modulus of 220 GPa and Poisson's ratio of 0.3. The MnS inclusion has Young' Modulus of 120 GPa and Poisson's ratio of 0.24. The stress-strain curves of

the steel and inclusion from [39, 16] are included in Appendix A; with the yielding strength of 100Cr6 is approximately 2300 MPa [39] and the MnS inclusion is 325 MPa [16].

3. Characterisation of subsurface microstructural damage

Microstructures of the spalled and indented areas of the upwind and downwind bearing raceways are investigated. The subsurface damages are evaluated by analysing observed inclusions, butterfly wing cracks, WEAs, and WEC networks. The following sessions present a detailed analysis of these damages.

3.1 Damaged inclusions

Fig.3 presents images of typical inclusion damage observed from the subsurface of the failed bearing raceways. In general, when an inclusion is perfectly bonded with the steel matrix, as shown in Fig.3a and Fig.3b, it is less likely to initiate the subsurface damage. However, when an inclusion is damaged by either boundary separation from the steel matrix or inclusion internal cracking, micro cracks initiate around these inclusions. Based on these observations, four different types of inclusion damage are identified.

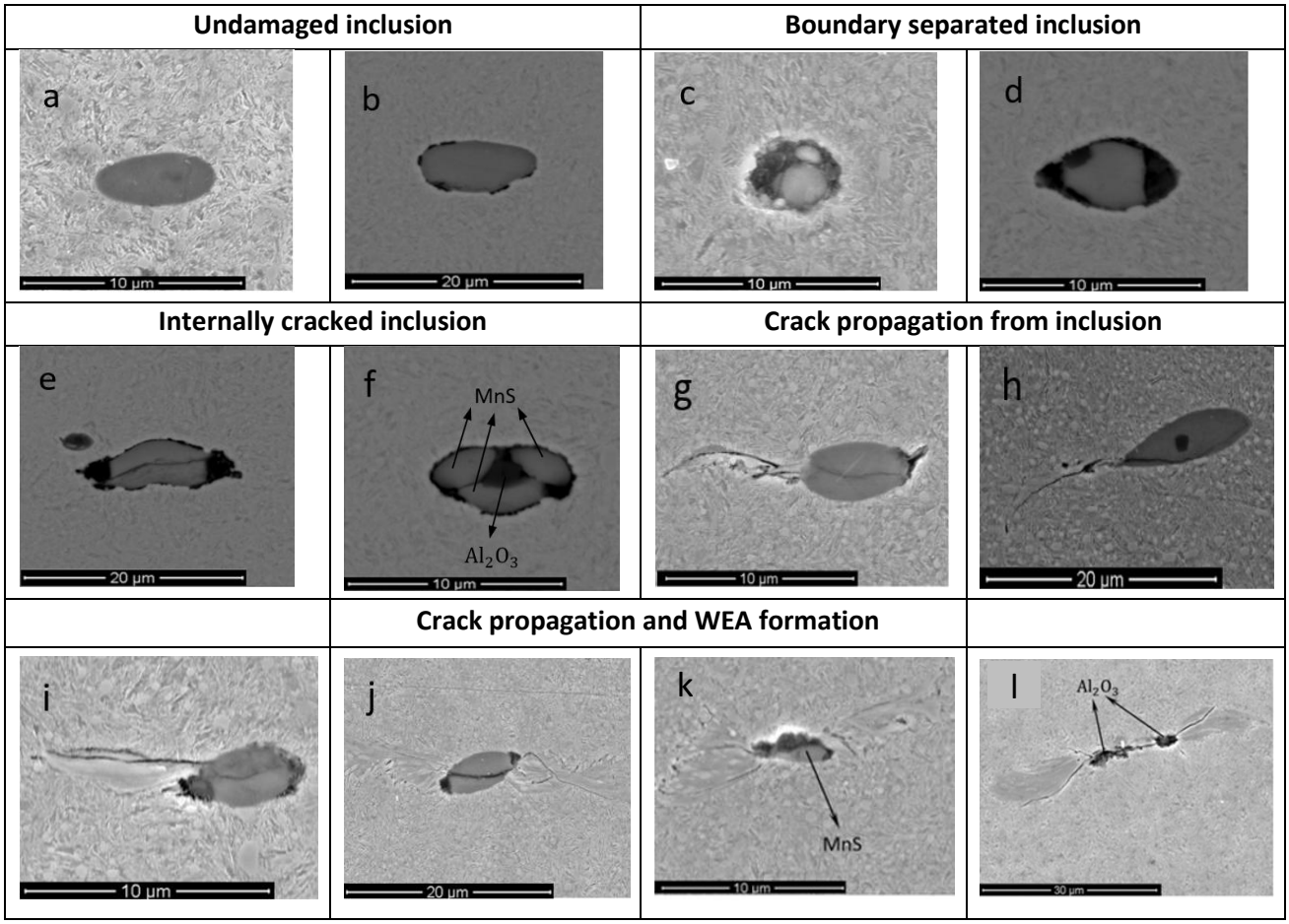

Fig.3 Different types of inclusion damage: (a) and (b) perfectly bonded inclusions; (c) and (d) boundary separation damage; (e) and (f) inclusions with internal cracks; (g) and (h) cracks propagated from inclusion into matrix; (i) (j) (k) and (l) butterfly cracks with WEA formation

The first damage type is the boundary separation of an inclusion, as shown in Fig.3c and Fig.3d. This type of the inclusion damage is most likely to occur during the steel heat treatment process because of differences in thermal expansion and contraction between the inclusion and steel matrix. In addition, the contact pressure acting on the raceway surface may also lead to boundary separation because the inclusion-matrix ionic bonds may be broken due to differences in deformation of the inclusion and steel. The second damage type is the internal cracking of an inclusion, as shown in Fig.3e and Fig.3f. The breakage of an inclusion is often caused by complex mechanisms. Firstly, the separation of the inclusion boundary from the steel matrix may occur due to the steel heat treatment or the loading from the rollers on the raceway. If the inclusion boundary is firmly connected to the steel matrix, energy from thermal expansion and contraction cannot be released through the debonding at the boundary. Hence, the relatively fragile inclusion may break internally itself because of its poor loading capacity. The other mechanism is related to the chemical composition of the inclusion. As shown in Fig.3f, in a compound inclusion of MnS+Al_2O_3, the MnS inclusion has been fractured into three pieces due to the Al_2O_3 particle located in the middle of the compound inclusion. Therefore, internal cracks may also initiate from the compound inclusions because of their fragile structures.

The third damage type is the internal crack propagation from an inclusion to the steel matrix, as shown in Fig.3g and Fig.3h. In this form of damage, the connection between the inclusion boundary and steel matrix is usually stable and firm. However, internal cracks of the inclusion may cause highly localised shear stress between the cracked surfaces during the subsequent RCF loading cycles. Therefore, the cracks may propagate from the inclusion into the steel matrix. Importantly, the cracks in the steel matrix caused by an inclusion are not only related to the internal cracks of the inclusion, but also influenced by any separated boundary or an excessive longitudinal ratio of the inclusion geometry. These factors also affect the maximum shear stress levels and cause the stress concentration localised at the inclusion when the raceway is subjected to a high contact pressure on the surface.

The fourth damage type is related to the WEAs at cracks around an inclusion, as shown in Figs.3i, 3j, 3k, and 3m. WEAs may form around the cracks due to sliding and impact loading between the fracture surfaces of these cracks [34]. Because the shape of the WEA damage is similar to butterfly wings, it is known as WEA “butterfly wing” damage. The investigation in [6] suggested that it was the final stage of the inclusion-initiated cracking. After the formation of WEAs at an inclusion, the local steel matrix transforms from martensite structure into a harder and more brittle ferrite structure. This undoubtedly provides favourable conditions for a rapid propagation of the cracks within the steel matrix under subsequent RCF cycles. Typically, the WEA associated cracks can propagate rapidly from the subsurface to the surface of the raceway and eventually cause the flaking of the surface material leading to spalling of the raceway.

3.2 Butterfly wing cracks and WEAs at inclusion

From the observation results within the subsurface of two failed bearing raceways (the damaged surface areas are shown in Figs.1b and 1c), a total of 114 butterflies with inclusions are found. The average length and the average width of the inclusions are 10.04 μm and 5.12 μm, respectively. Cleanliness tests show that MnS inclusions exceed 90% of all inclusions observed and more than 89% of butterfly wing cracks are associated with MnS inclusions. The butterflies are more likely to be found in the circumferential samples than in the axial samples of the raceways. They are clustered in the middle section of the spalled raceway surface, in both upwind and downwind raceways, shown in Figs.1b and 1c. This is because the circumferential samples are aligned with the rolling contact direction, butterfly wings are affected by surface traction in the circumferential direction, greater than that in the axial direction of the bearing.

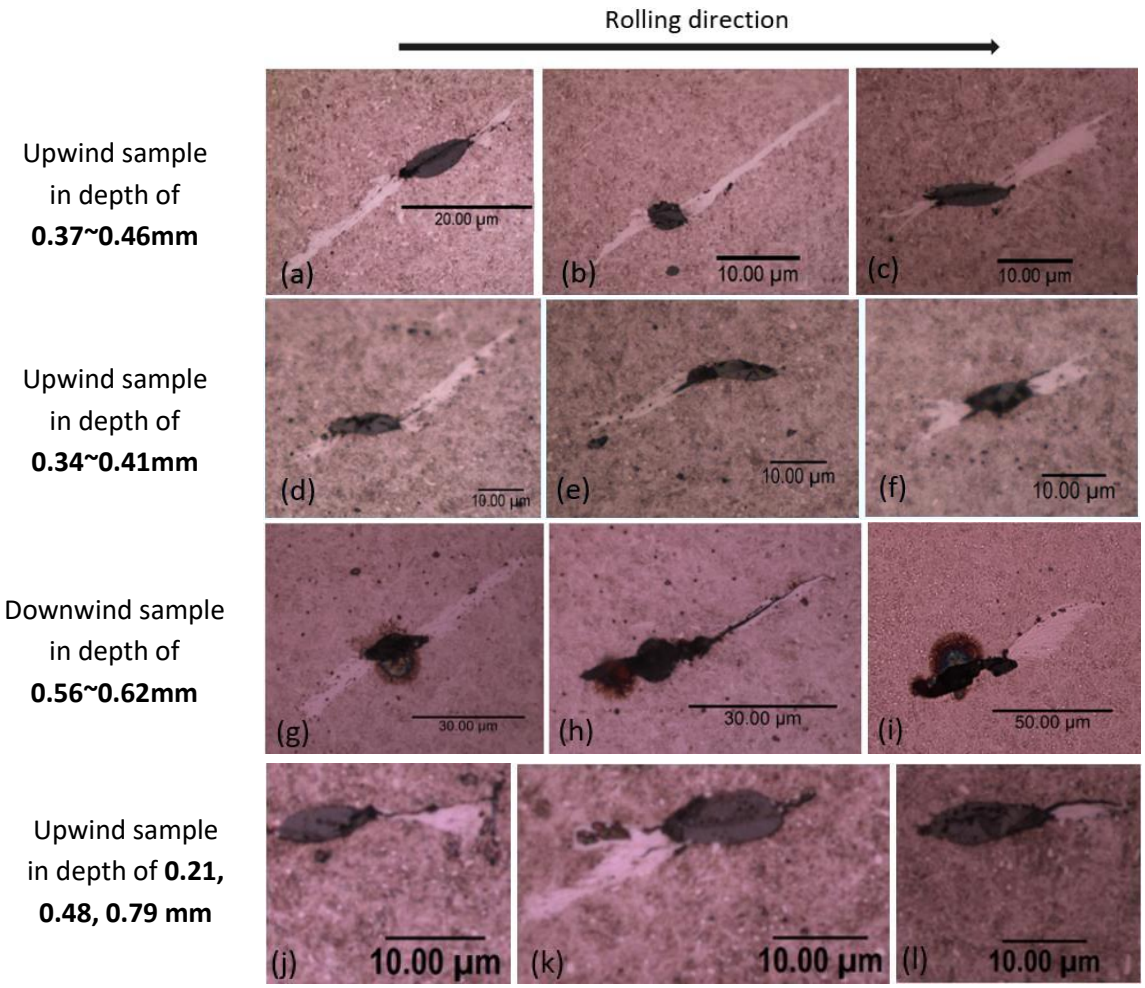

Fig.4 Butterfly wing cracks and WEAs at inclusions located at different depths in subsurface

To investigate factors affecting the propagation direction of butterfly wing cracks, Fig. 4 shows some examples of butterfly wing cracks and WEAs at inclusions from circumferential and axial samples. From Figs.4a,b,c, though these three butterflies are found at similar subsurface depths in the same sample, the geometry and inclined angles of their inclusion are completely different. However, the WEA decorated butterfly wings propagated from the inclusion are almost in the same direction, at an acute angle to the rolling direction. Similar observations can be found from different samples in Figs.4d,e,f and Fig.4g,h,i, when the butterflies are at the similar depths, their WEA decorated

butterfly wings propagate in the similar direction. However, when inclusions are located at different subsurface depths of 0.21, 0.48 and 0.79 mm, the WEA decorated butterfly wings propagate in different directions, as shown in Fig.4j,k,l.

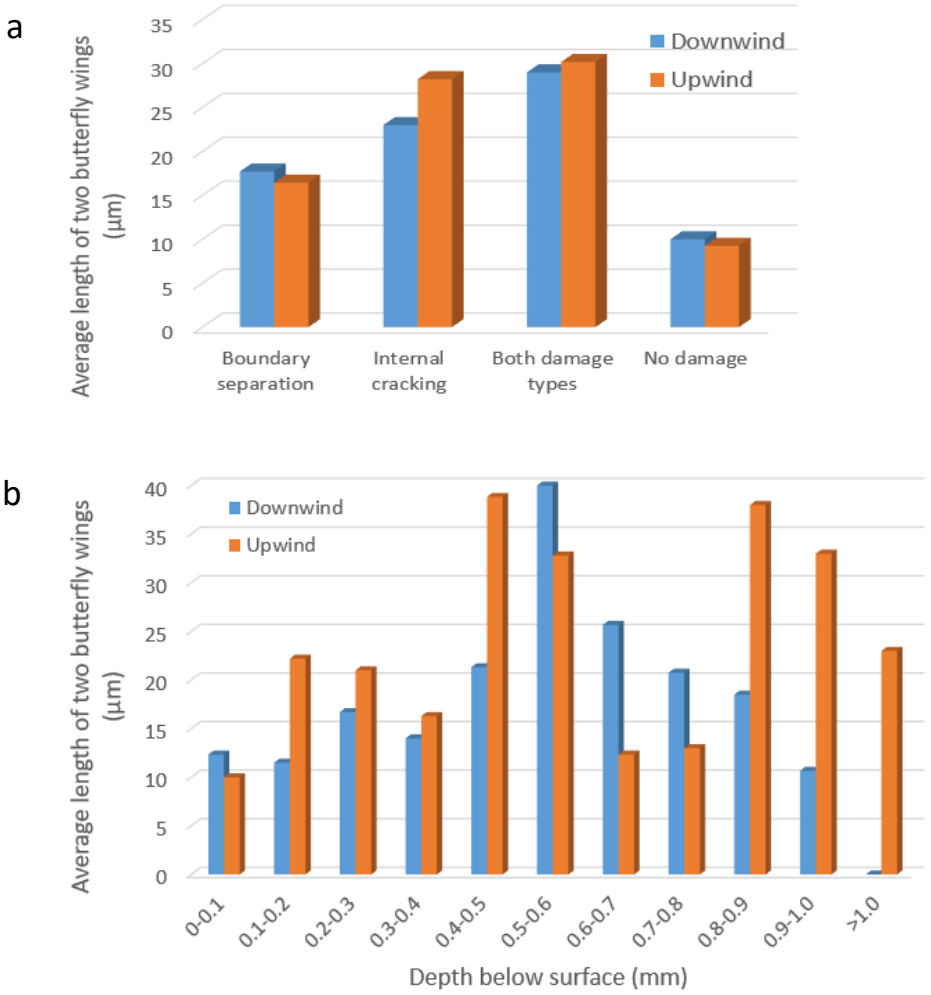

Fig.5 Average crack length of butterfly wings at inclusion: (a) Effect of inclusion damage types on crack length; (b) Correlation of crack length with subsurface depth

Statistical analysis of the subsurface damage results, based on all inclusions found in the subsurface of the damaged raceways, is conducted by relating the inclusion damage types to the average length of butterfly wing cracks at an inclusion, as shown in Fig.5a. Because internal cracks and boundary separations of inclusions can be found in the subsurface area at varied depths, the results of the statistical analysis are processed to show the correlation of crack lengths of the butterfly wings with the subsurface depth. It can be observed that the most harmful inclusion damage types to the raceway subsurface are the internal cracking and boundary separation of inclusions. It has been found that when an inclusion has both damage types, it creates the greatest average crack lengths of the butterfly wings, propagated from the inclusion. If only one damage type exists at an inclusion, the internal cracking of the inclusion has been found to be more harmful than the boundary separation of the inclusion.

Most butterflies are found to be located in the subsurface depth from 0.2 to 0.6 mm, as shown in Fig. 5b. It can be seen that the average length of the butterfly wings increases first with the increased depth but decreases towards greater depths. The maximum butterfly lengths are within the subsurface depth of 0.4 to 0.6 mm. However, longer butterfly wing cracks are also observed in the downwind raceway reaching to the subsurface depth of 1 mm from the contact surface. This may be related to the change in the contact area caused by surface spalling of the raceway, which in turn leads to higher stresses of the contact area. Section 4 will present FE stress analysis to explain these observations.

3.3 Subsurface crack networks and WEAs

In this study, it has been observed that most subsurface cracks are initiated from inclusions in the raceway subsurface. If an inclusion has either boundary separation or internal cracking or both damage types, it is most likely to initiate micro cracks around the inclusion, providing nucleation sites for them to connect and to form a large crack network. As shown in Fig. 6, these inclusions appear as small black dots within the crack networks. The orientation of the crack networks is different in the axial and circumferential samples cut from the raceways; most of the cracks of the axial samples are directed horizontally but the cracks of the circumferential samples are mostly directed at an angle of 15~30 degrees to the contact surface of the raceway. Some of these circumferential crack networks have propagated to the contact surface and/or have connected with other crack networks, as shown in Fig.6c and Fig.6d.

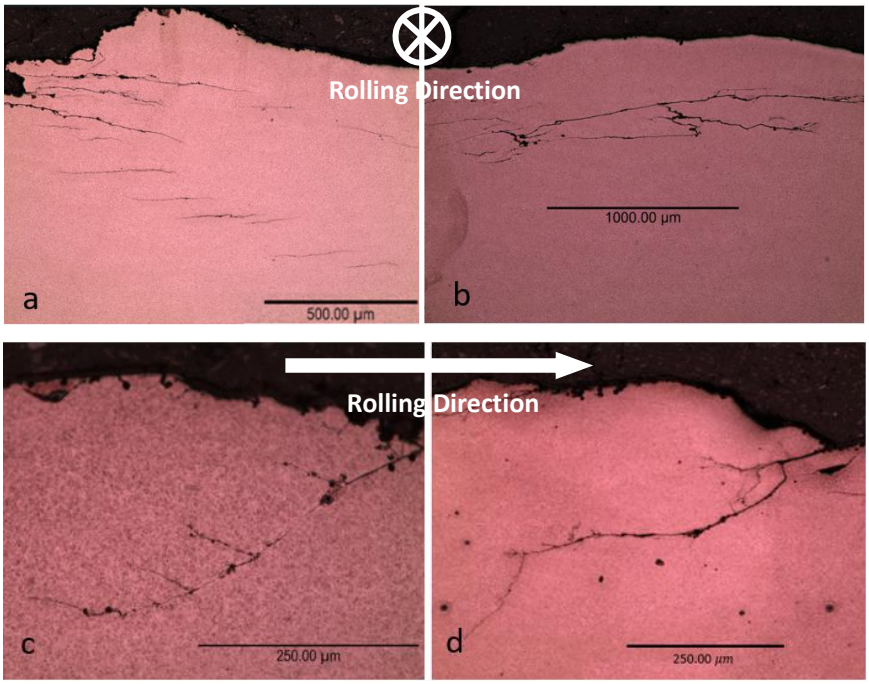

Fig.6 Subsurface crack networks: (a) upwind axial sample; (b) downwind axial sample; (c) upwind circumferential sample; (d) downwind circumferential sample

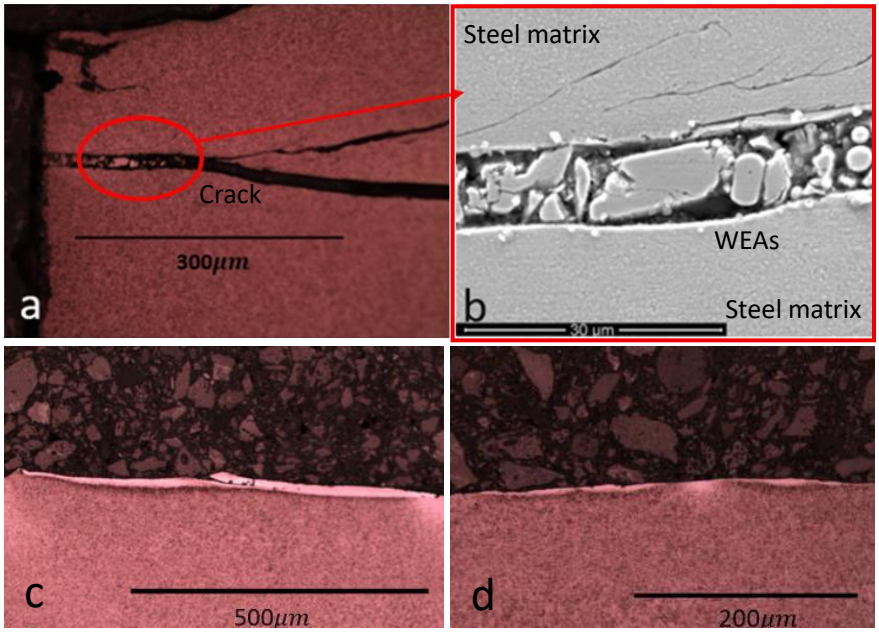

Fig. 7 White etching crack (WEC) networks: (a)(b) optical and SEM image of broken WEAs within crack from downwind axial sample; (c)(d) white surface flaking from upwind axial samples

Many investigations of the bearing premature failure showed that the bearing surface spalling was initially triggered by WECs from the subsurface areas [3, 8, 13, 35, 40]. Fig. 7a shows a WEC network observed from a downwind axial sample; some broken WEA particles are found entirely within the crack in the subsurface which is parallel to the raceway surface. The microstructure difference between the original steel matrix and WEAs is clearly shown in Fig.7b. The broken areas surrounded by WEAs in the crack have smooth surfaces, which means no carbide can be observed. However, for the steel matrix above and below the crack, it exhibits a frosted texture because there are spherical carbide particles within the steel matrix. Two examples of the white structure flaking (WSF) observed from the spalled raceways are shown in Figs. 7c,d. The steel material above the WEC has already been flaked away, thus only the cracks with decorated WEAs remain on the observed sample surface; some of the WEAs are also broken and cracked, similar to that observed in Fig.7a.

A large number of WEAs due to inclusions is observed in this study, and this type of WEAs is often accompanied by the micro cracks within the butterfly wings in the subsurface. However, WEAs without being attached to any inclusion are also observed in the raceway samples. These WEAs are often found in the subsurface crack networks and surrounded by longer cracks, examples of these WEAs are shown in Fig. 8. To confirm whether these WEAs are caused by inclusions, the current observation plane of the sample surface is subjected to an additional polishing process, followed by an etching process, aiming to investigate whether any inclusions still exist beneath the current observation plane. However, the crack network geometries remain unchanged after observing three different planes of the sample, indicating that these WEAs may not be caused by subsurface inclusions.

Fig. 9 shows a WEC network found from a downwind sample; no inclusions can be observed from the WEC and the crack has propagated to deeper region in the subsurface, approximately 5 mm below the spalled surface of the raceway, indicating there may be other possible factors contributed to the complex crack networks in the subsurface of the failed raceways.

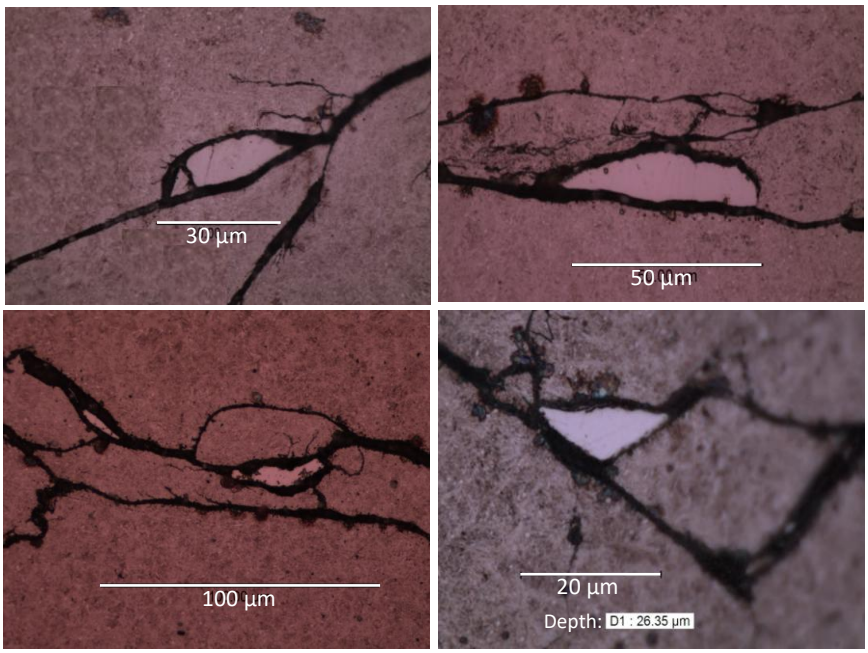

Fig. 8 Subsurface crack networks without attached to any inclusions

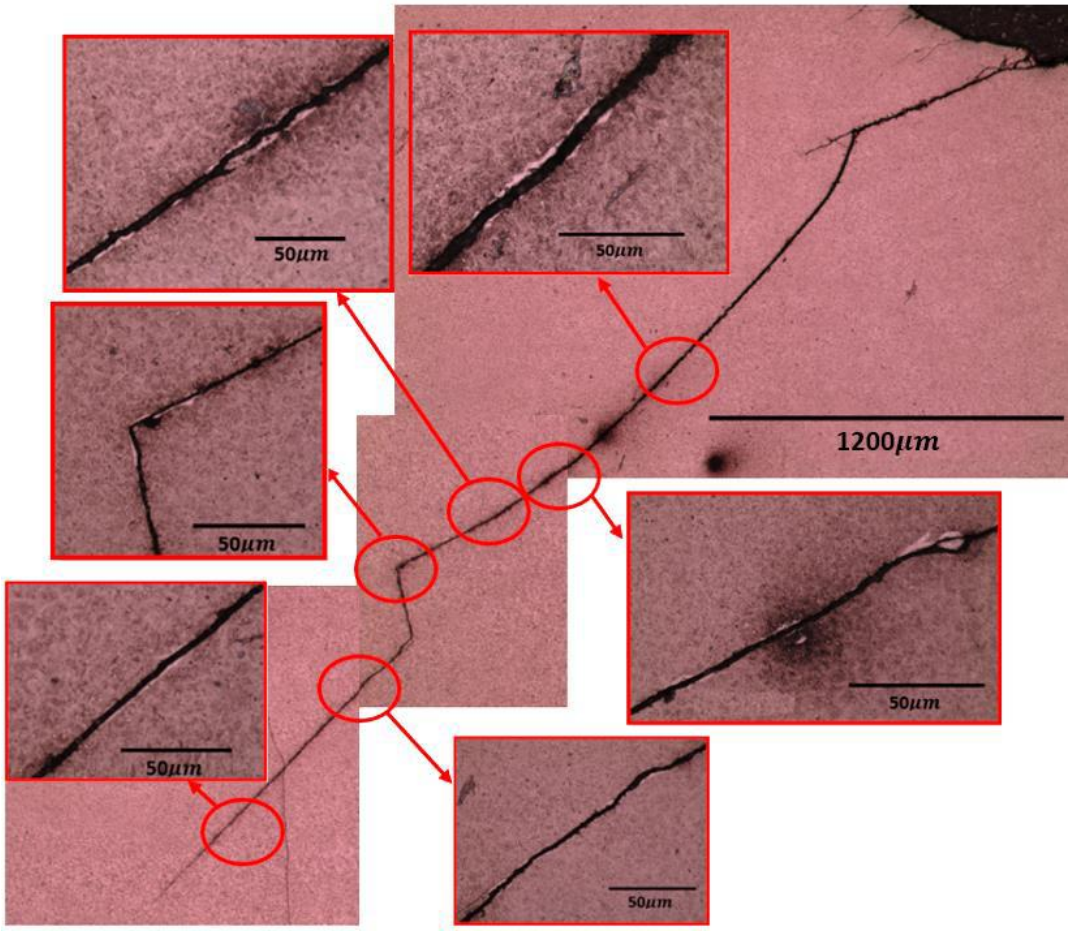

Fig.9 WEC network propagated into deeper subsurface at 5 mm from the raceway contact surface

To ascertain the formation of the subsurface crack networks is initiated from the raceway subsurface, the subsurface microstructure of the raceway surface without flaking or spalling damage but only with indents, as shown in Fig. 1c, is also investigated. Away from the fixed loading zone of the raceway, no subsurface crack networks can be found beneath the surface without flaking or spalling damage. However, four butterfly wing cracks at inclusions in the subsurface are still detected in circumferential samples; all of them are caused by either boundary separation or internal cracking of the MnS inclusions, as shown in Fig. 10. This observation confirms that the subsurface crack networks are initiated from the damaged inclusions within the subsurface.

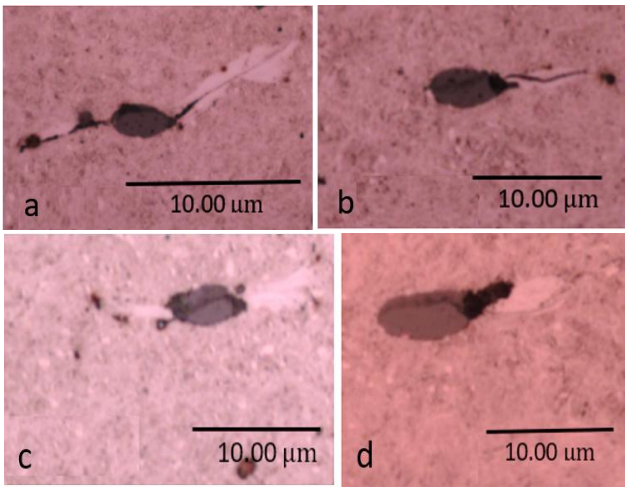

Fig.10 Butterfly wing cracks with WEAs at MnS inclusions of the subsurface of indented downwind raceway without surface flaking or spalling

4. Discussion of formation mechanism of WEAs and WECs

From the microstructure damage investigation presented in the previous section, extensive butterfly wings with micro cracks and WEAs at MnS inclusions are found in the subsurface of the damaged raceways. Long crack networks with WEAs and WECs are also observed in the raceway subsurface connected to surface flaking and spalling, while some WECs have propagated into deeper regions of the subsurface of the raceways. In the following subsections, the damage initiated at inclusions leading to the formation of butterfly wing cracks, WEAs and WECs, and secondary cracks in the subsurface will be discussed.

4.1 Initiation of butterfly wings with micro cracks at damaged inclusion

The developed global FE model has produced results of subsurface stress variations when the roller moves over the raceway surface. Fig. 11 shows how the Tresca stress varies over one rolling contact loading cycle without considering an inclusion in the subsurface. In Abaqus, the Tresca stress is defined as two times of the maximum shear stress. The maximum stress is located at the subsurface depth around 0.4 mm and an elevated stress zone in the subsurface covers the subsurface depth from 0 to 1.6 mm. Considering the bearings would undergo millions of loading cycles in operation, any inclusions located in these subsurface areas will experience varied stress conditions which result in fatigue damage to both the inclusions and the steel material surrounding them.

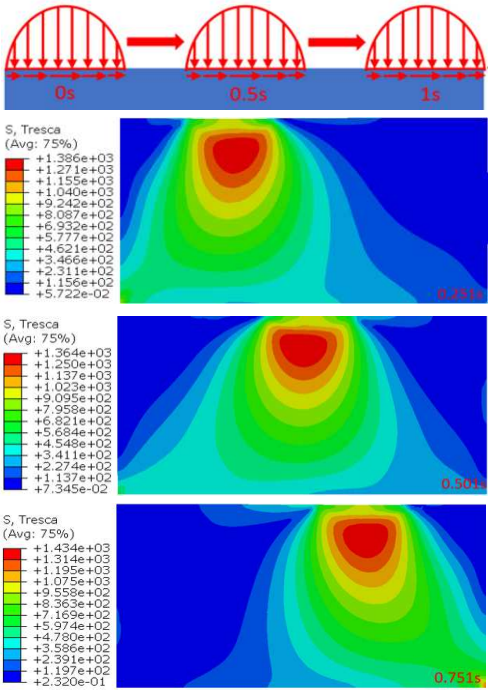

Fig. 11 Variation of Tresca stress under one rolling contact cycle: roller located at left (0.251s), centre (0.501s) and right (0.751s) of the raceway surface

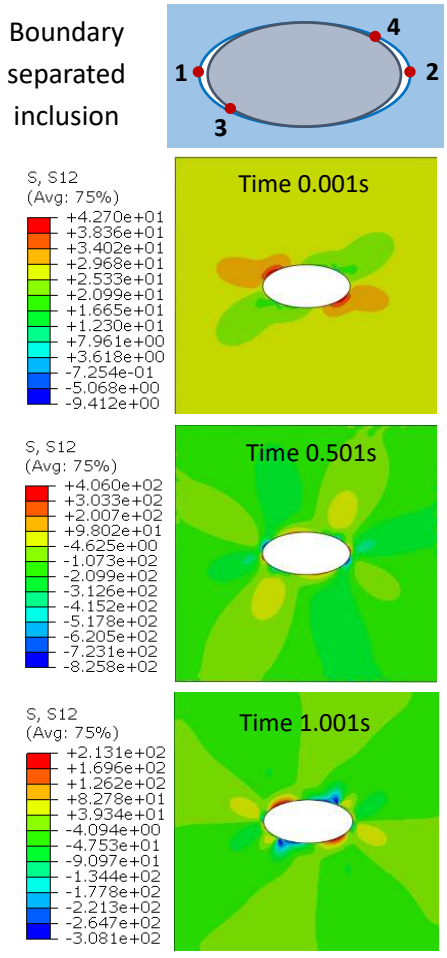

Fig. 12 Variations of orthogonal shear stress of boundary separated inclusion (four locations of highest stress variations are highlighted) when roller at far left (0.001s), centre (0.501s) and far right (1.001s) on raceway surface

In addition to the rolling contact cycle induced stress variations in the subsurface, the existence of inclusions causes stress concentration and further stress variations around the inclusions. The developed FE sub-model of an inclusion has investigated three different conditions of the inclusion: undamaged, boundary separated and internal cracked, as observed in Section 3.1. In the boundary separation model, the friction coefficient between the steel matrix and inclusion is defined as zero; this is because MnS can reduce interfacial friction when its size is typically small. In the initial state of the FE model, the tips of the inclusion are separated from the steel matrix, but the middle part of the inclusion is connected with the matrix. In the internal crack model, the inclusion is defined as perfectly bonded with the matrix. The contact between the cracked surfaces of the inclusion is set as frictionless, considering the low friction level of the small MnS inclusion considered in the model.

The FE modelling results show for each condition of the inclusion when the roller moves over the raceway surface in one roller contact cycle, points 1~4 of the steel material immediate to the inclusion experience highest variations of the orthogonal shear stress, as shown in Fig. 12. Fig.13 shows a comparison of variations of the orthogonal shear stress at point 3 of the steel matrix due to different inclusion conditions. It can be seen that the maximum stress variation range of the internally cracked inclusion is 1629 MPa (from −933 MPa to 696 MPa), greater than 1516 MPa (from −614 MPa to 902 MPa) for the boundary separated inclusion. For the undamaged inclusion, the maximum stress variation range is less than 1000 MPa (from −576 MPa to 400 MPa).

The FE stress modelling results support the observation of extensive subsurface butterfly wing damage observed from the failed bearing raceways, as shown in Figs. 3, 4, and 10. The majority of these butterflies are found at inclusions located in the depth of 0.4 mm to 0.6 mm, deeper than the modelled depth of the maximum shear stress at 0.4 mm. Considering the flaking / spalling damage of the contact surface of the raceways, the actual contact pressure may be much higher than the rated condition (2.069 GPa) modelled in this study due to the uneven surfaces after the occurrence of flaking / spalling damage. Higher contact pressure increases the depth of the maximum shear stress, as well as the length of butterfly wings in the deeper subsurface region. Repeated large variations of the orthogonal shear stress at the damaged inclusions, both internal cracking and boundary separation, significantly increase the risk of initiating fatigue cracks at critical locations of the inclusion (points 1~4), similar to that observed in the microstructure damage of the butterfly wing cracks. With multiple inclusions in the subsurface, micro cracks propagating from various inclusions can form crack networks in the subsurface.

Orientations of micro cracks of each butterfly at different subsurface depths can be different, as evidenced in Fig. 4. This is because the depth difference of inclusions results in the difference of the orthogonal shear stress distribution and variation around each inclusion. Therefore, under repeated rolling contact cycles, developed fatigue cracks at butterflies have diverse geometries and crack orientations. In the actual operation of a WT, a bearing raceway can be subjected to different levels of contact loading and surface traction; affecting crack propagations along both circumferential and

axial directions of the bearing. The surface traction of the cyclic movement of the bearing rollers mainly affect shear stresses in the circumferential direction, without considering misalignments. Therefore, the propagation of circumferential cracks is mostly directed at an angle of 15~30 degrees to the rolling direction of contact surface of the raceway; while axial cracks approximately propagate parallelly to the bearing raceway axis, as observed in Figs. 4 and 10.

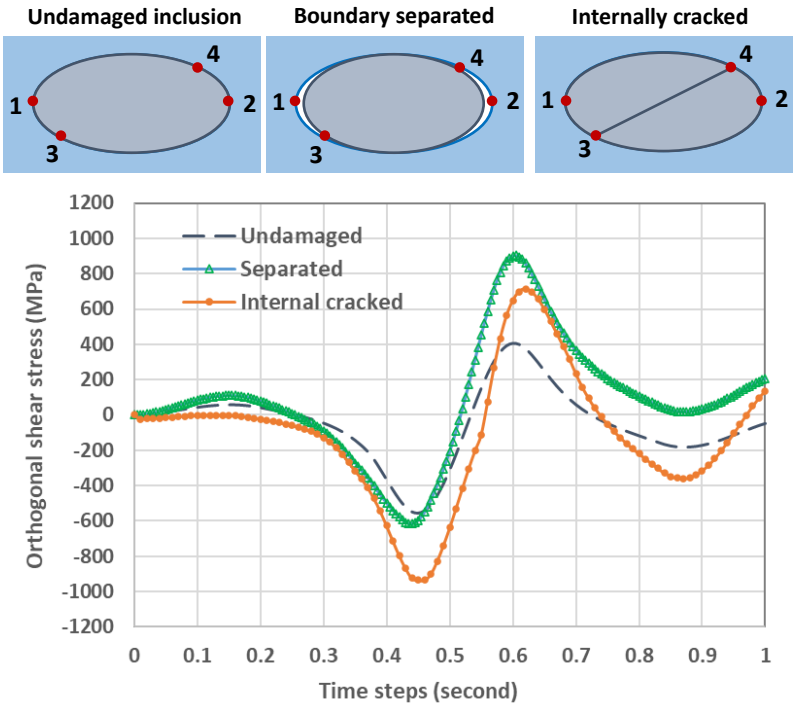

Fig.13 Variations of the orthogonal shear stress caused by different inclusion conditions

4.2 Formation mechanisms of white etching areas

The microstructure of WEAs was identified as the nanocrystalline ferrite that was supersaturated with carbon [41, 42]; and the grain sizes of the WEAs were reported to be ranged from 20 to 30 nm [43]. To investigate the microstructure differences between WEAs and the original martensitic structure, a WEA on a crack in an axial sample from the surface flaking area is investigated by using SEM, as shown in Fig.14. Four regions are selected; Zone 1 is the WEA; Zone 2 shows the microstructures on both sides of the crack; Zone 3 is the original martensite structure of the steel; and Zone 4 is the microstructure of the transition zone from the martensite to the WEA which locates below the crack.

As can be seen from Zone 3, the martensite in the original structure has a needle-shaped structure. Because carbon is added during the steel manufacturing, some circular carbides, with the chemical composition M_3C, can also be observed around the acicular martensite. In general, the carbides will absorb some of Fe element to form Fe_3C, named as cementite. Comparing the images of four zones in Fig.14, it can be seen that the circular cementite disappears in the microstructure of the WEA in Zone 1. Although the cementite can still be found in the transition region of Zone 4, they become extremely rare in the WEA in Zone 1. This can be seen more clearly in Zone 2, where the distribution of cementite is mainly concentrated in the region below the crack.

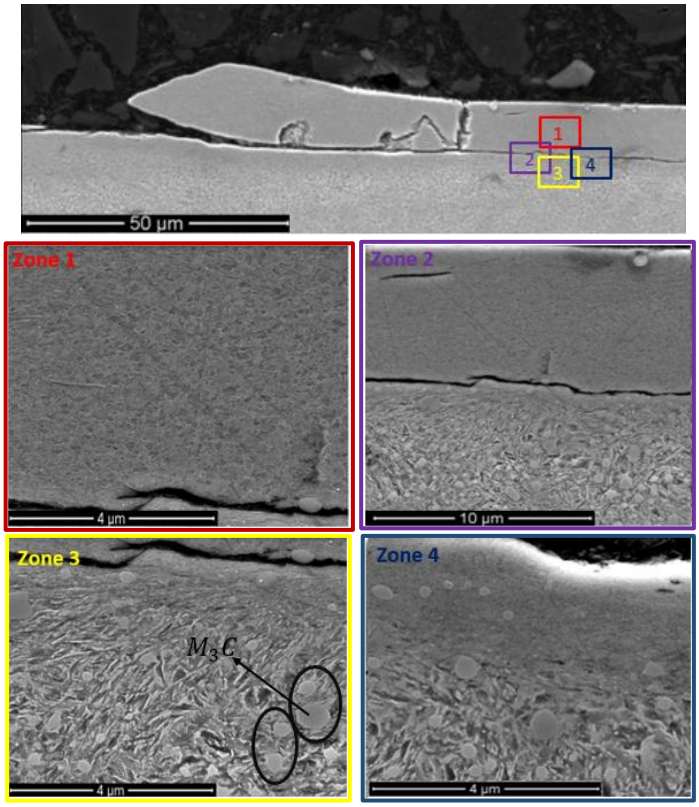

Fig.14 Comparison of microstructures of WEA and original martensite

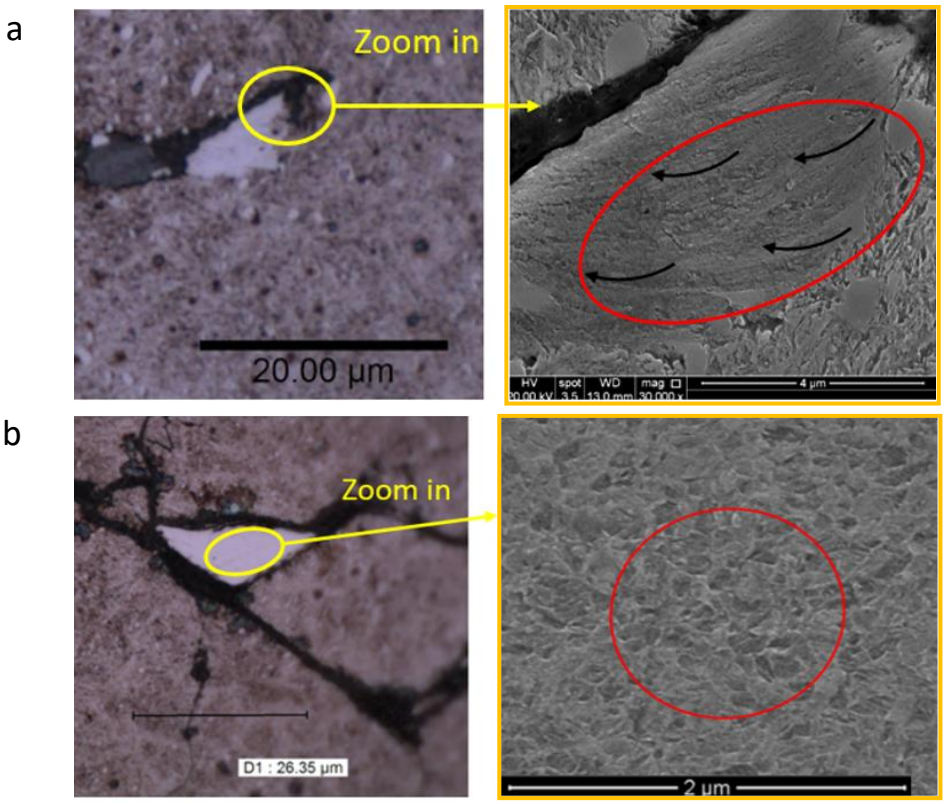

Fig.15 WEAs in butterfly wing cracks from circumferential samples of upwind raceway: (a) with elongated cementite; (b) without elongated cementite (the enlarged images are on the right)

The investigation in [9] attributed the disappearance of cementite in the WEA to the effect of the shear stress on the formation of butterfly wing cracks. Due to the high strain-rate shear deformation,

elongated cementite can be broken up and dissolved during subsequent rolling contact loading cycles. From this study, elongated cementite elements can be observed in the butterfly wing cracks from a circumferential sample of the upwind raceway, shown in Fig.15a. However, in this study, not all the WEAs are found to contain the elongated grains in the microstructure. An explanation in [44] suggested that there might exist a thermal-mechanical mechanism that resulted in the dissolution of the cementite because an increase of temperature of the microstructure was observed during the WEA formation process. Furthermore, the interaction between the dislocated grain boundary and the cementite might also lead to the damage and dissolution of the cementite, as reported in [45].

From the microstructure of another circumferential sample of the upwind raceway shown in Fig.15b, a WEA is observed alongside a crack network in the subsurface area. From the SEM image shown on the right, it is clear that the microstructure of this WEA is the compact ferrite without the elongated grains, highlighted by a red cycle. Moreover, the boundaries of the grains in Fig.15b are clearer than those in Fig.15a. These differences may be because under the rolling contact loading, the triangular WEA in Fig. 15b, surrounded and in contact with three cracked surfaces of the crack network, is subjected to shearing deformation applied to the area in three different directions. Accordingly, the interactions between the grains in Fig.15b is multidirectional, which may be the main reason for the formation of dense ferrites. However, for the WEA in Fig.15a, it only has one surface interacting with the butterfly wing crack, under the rolling contact loading, the WEA is only subjected to one dimensional shear deformation affecting the formation of ferrite grains, mainly oriented along the crack direction of the butterfly wing. This confirms that the formation of WEAs is caused by a variety of mechanisms, not only due to the existence of damaged inclusions.

4.3 Formation mechanisms of WECs and secondary cracks

In addition to the observation of extensive WEAs attached to micro cracks of the butterfly wings at inclusions, the long crack networks surrounded or decorated by WEAs in the subsurface, termed as WECs, are also observed, such as those shown in Figs. 7 and 9. The formation of subsurface crack networks and WECs is observed to be the most harmful magnification of the subsurface damage, eventually leading to the final failure of the bearings.

A few studies suggested that WECs were initiated by butterfly wing damage, voids or other subsurface defects [21, 33, 34, 35]. In this study, it has been found that the butterfly wing cracks connect with each other in the subsurface area to form the WEC networks. However, some studies did not observe any inclusions within the WECs, indicating that the formation of WECs could be independent of inclusions [36, 37]. Currently there were three main hypothesised mechanisms of the formation of WECs [21]. The first hypothesised mechanism was the rubbing theory of cracked surfaces, which suggested that two surfaces of an existing crack could rub against each other under cyclic loading. The accumulated friction energy could lead to the atom dislocations of the steel matrix, and eventually the formation of WEAs on the crack. This formation mechanism may be similar to the growing process of WEAs of the butterfly wings at damaged inclusions. The second hypothesised mechanism was related to the Adiabatic Shear Bands (ASB) theory [26]. It considered that the impact

loading could lead to the high strain rate deformation and subsequent heating of the steel material in localised areas, making it easier for the microstructure to transform from martensite to ferrite [19]. The last hypothesised mechanism suggested that the lubricant could enter cracked gaps to generate electrical discharges under certain conditions. Accordingly, the local areas may be heated and corroded by the electrothermal effect, leading to the initiation of WEAs on the crack [8].

Fig. 7 shows examples when the steel material above the WECs has already flaked away, thus only the cracks with decorated WEAs can be observed; where some of the WEAs are also fractured. It can be seen that the WEA does have the finer grains compared with the original martensite matrix. This is because the hardness of WEAs is 30% to 50% higher than that of the martensitic structure [46], the ductility and toughness of WEAs are lower than the martensite, thus the WEAs are prone to be cracked and shattered. Under subsequent rolling contact loading cycles, the surface areas where flaking or spalling already occurred may be further hardened, causing further surface flaking and spalling damage. In addition, when the surface material has already flaked away, the damaged surface material may be directly in contact with the lubricant, which could lead to localised hydrogen embrittlement. Undoubtedly, both the strain hardening and hydrogen embrittlement may further reduce the ductility of the already damaged surface material. When higher contact loads occur, such as under impact loading, the secondary cracks may form beneath these spalled surface areas into deeper regions of the subsurface, accelerating crack propagation which leads to the final failure of the bearings.

Similar to the subsurface micro cracks initiated from inclusions, the secondary cracks may also contain WEAs. The WEC crack network shown in Fig.9 is observed in the circumferential direction of the raceway. Because no inclusions can be found associated with the crack network, which has propagated into the deeper region below the spalled surface, this crack network is identified to be a secondary crack. At the depth of 5 mm where the crack network is propagated to, the stress magnitude caused by the contact pressure at the raceway is typically small. Therefore, the formation of WEAs in the WEC crack shown in Fig.9 could not be caused by the damage initiated at inclusions due to cyclic stress alternation. There may be three possible explanations for the WEA initiation process in the secondary cracks. Firstly, lubricant may leak from the contact surface into the subsurface alongside the secondary crack to the deeper region in the subsurface, resulting in the localised electrical current discharge and heating. Secondly, WEAs may easily form due to the localised shearing and heating if these areas are adiabatic, according to the ASB theory. Thirdly, the rubbing and squeezing between the cracked surfaces under cyclic rolling contact may lead to the accelerated recrystallisation of the steel matrix from martensite to ferrite. All these possible mechanisms suggest that the WEAs could have formed after the occurrence of the crack network, considering the subsurface depth of this crack network. Compared with the WECs observed in Fig.7, the area of WEAs of the WEC in Fig.9 is relatively small. This may be because the secondary crack network has occurred after the spalling of the raceway surface, thus the formation period of WEAs in Fig.9 is relatively short, when compared with the WEAs formed at subsurface micro cracks initiated from inclusions in Fig.7.

Based the evaluation of the microstructural damages presented in Sections 3.1, 3.2, and 3.3 as well as the discussion of the damage initiation and propagation mechanisms presented in Sections 4.1, 4.2 and 4.3, this study concludes that the failure of the two bearing raceways is initiated from the subsurface. A damage progression hypothesis of the failed bearing raceways is proposed, including six stages, as shown in Fig.16. It can be concluded that the butterfly wing cracks at damaged inclusions is the original cause of the raceway failure. Due to the propagation of micro cracks and the formation of WEAs of the butterfly wings at damaged inclusions, the WEC networks are formed and propagated to reach the raceway surface to cause white structure flaking. The following RCF loading cycles result in the formation of further secondary WEC networks in greater subsurface depths and severe damages to the surface, leading to the final spalling failure of the raceways.

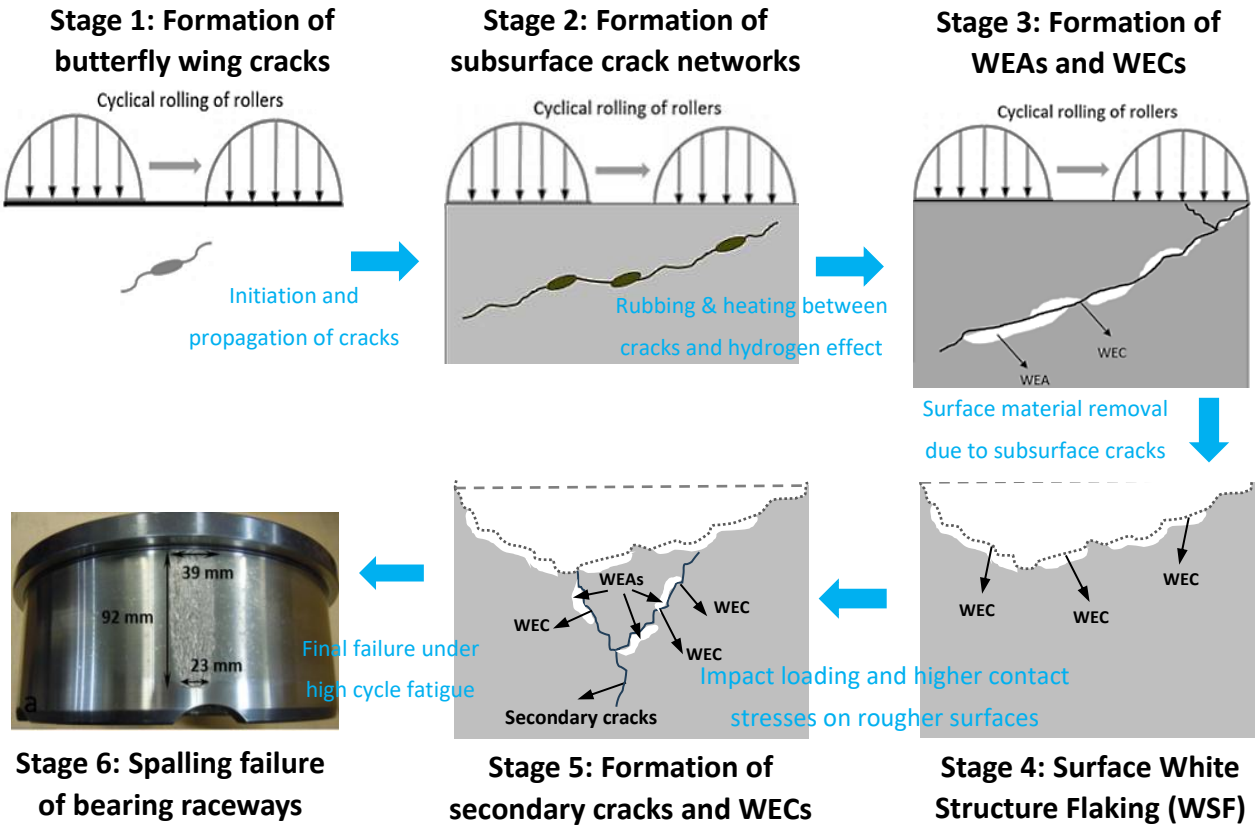

Fig.16 Damage progression of bearing raceways under rolling contact fatigue

5. Conclusions

In this study, damage characterisation and evaluation by employing optical microscope and SEM, and FE stress analysis under rolling contact loading condition are conducted to investigate the microstructural damage of the failed WT gearbox bearings. The study identifies butterfly wing cracking, WEAs and WECs, and secondary cracks and proposes a new hypothesis of damage progression which leads to the premature failure of the bearings. The key conclusions can be drawn:

1) When inclusions in the subsurface are damaged by separated boundaries and/or internal cracks, the risk of crack initiation and propagation at those inclusions increases greatly. An internal

cracked inclusion is generally more harmful than an inclusion with boundary separation; because of increased average crack lengths of butterfly wings from the inclusion.

2) Subsurface crack networks are observed and the average length of these crack networks is generally less than 1 mm, and inclusions are found to be the connections between the shorter cracks. It can be concluded that these crack networks are generated by the propagations of the micro cracks at butterfly wings initiated by multiple inclusions.
3) WEAs are found in micro cracks of the butterfly wings and the subsurface crack networks to form WECs. Some WEAs are generated by the subsurface inclusions, while some are affected by the cracked surfaces within the subsurface crack networks. It is clear that the formation of the WEAs involves the dissolution of the cementite and the transformation of the steel microstructure from martensite to ferrite, although the initiation causes of the WEAs are different.
4) Due to the higher hardness and poor ductility of WEAs, some of them are fractured under subsequently repeated rolling contact loading cycles. Therefore, the damage of the subsurface areas is intensified, leading to the accelerated material flaking and spalling of the contact surface of the bearing raceways, eventually leading to the bearing premature failure.
5) Following the occurrence of the raceway material flaking or spalling, some secondary cracks are formed in deeper regions of the subsurface due to the impact loading or higher stresses occurring on flaked and spalled surfaces of the raceway. In some cases, WEAs may form after the occurrence of the secondary cracks, because of interaction of the cracks with lubrication, and thermal-mechanical effects between the cracked surfaces.
6) The damage progression hypothesis of the failed bearing raceways can be concluded to include six stages. The butterfly wing cracking at damaged inclusions is the original cause of the raceway failure. It leads to the propagation of micro cracks and the formation of WEAs at the butterfly wings to form the subsurface WEC networks. These crack networks are propagated to reach the raceway surface to cause white structure flaking, which results in further secondary crack networks and WECs, leading to the final spalling failure of the bearing raceways.

CRediT Author Statement

R. Dai: Conceptualisation, Methodology, Investigation, Formal Analysis, Validation, Visualization, Writing – original draft, Writing – review and editing.

H. Long: Conceptualisation, Methodology, Supervision, Funding acquisition, Writing – original draft, Writing – review and editing.

Declaration of Competing Interest

The authors declare that they have no known competing interests for the publication of the work reported in this paper.

Acknowledgments

The authors wish to acknowledge the support of our anonymous partner for the provision of the failed bearings.

References

[1] H. K. D. H. Bhadeshia, “Steels for bearings,” Prog. Mater. Sci., vol. 57, no. 2, pp. 268–435, 2012.

[2] Z. Liu, Y. Bao, M. Wang, X. Li, and F. Zeng, “Austenite grain growth of medium-carbon alloy steel with aluminum additions during heating process,” Int. J. Miner. Metall. Mater., vol. 26, no. 3, pp. 282–290, Mar. 2019.

[3] H. A. Al-Tameemi, H. Long, and R. S. Dwyer-Joyce, “Damage characterisation of white etching cracks in a black oxide coated wind turbine gearbox bearing,” Wear, vol. 432–433, p. 102923, 2019.

[4] C. Gu, M. Wang, Y. Bao, F. Wang, and J. Lian, “Quantitative Analysis of Inclusion Engineering on the Fatigue Property Improvement of Bearing Steel,” Metals (Basel)., vol. 9, no. 4, p. 476, 2019.

[5] Y. Wang, A. Karasev, J. H. Park, and P. G. Jönsson, “Non-metallic Inclusions in Different Ferroalloys and Their Effect on the Steel Quality: A Review,” Metall. Mater. Trans. B 2021 525, vol. 52, no. 5, pp. 2892–2925, Jul. 2021.

[6] J. Maciejewski, “The Effects of Sulfide Inclusions on Mechanical Properties and Failures of Steel Components,” J. Fail. Anal. Prev., vol. 15, no. 2, pp. 169–178, Apr. 2015.

[7] K. Gillner, M. Henrich, and S. Münstermann, “Numerical study of inclusion parameters and their influence on fatigue lifetime,” Int. J. Fatigue, vol. 111, pp. 70–80, Jun. 2018.

[8] A. D. Richardson, M. H. Evans, L. Wang, R. J. K. Wood, M. Ingram, and B. Meuth, “The Evolution of White Etching Cracks (WECs) in Rolling Contact Fatigue-Tested 100Cr6 Steel,” Tribol. Lett., vol. 66, no. 1, pp. 1–23, 2018.

[9] T. Bruce, E. Rounding, H. Long, and R. S. Dwyer-Joyce, “Characterisation of white etching crack damage in wind turbine gearbox bearings,” Wear, vol. 338–339, pp. 164–177, 2015.

[10] T. Bruce, H. Long, and R. S. Dwyer-Joyce, “Threshold Maps for Inclusion-Initiated Micro-Cracks and White Etching Areas in Bearing Steel: The Role of Impact Loading and Surface Sliding,” Tribol. Lett., vol. 66, no. 3, 2018.

[11] G. H. Jiang, S. X. Li, J. Bin Pu, and F. Yu, “Phase transformation in the subsurface of case carbonitrided bearing steels under rolling contact fatigue,” Tribol. Int., vol. 169, p. 107468, May 2022.

[12] M. H. Evans, J. C. Walker, C. Ma, L. Wang, and R. J. K. Wood, “A FIB/TEM study of butterfly crack formation and white etching area (WEA) microstructural changes under rolling contact fatigue in 100Cr6 bearing steel,” Mater. Sci. Eng. A, vol. 570, pp. 127–134, May 2013.

[13] H. A. Al-Tameemi, H. Long, and R. S. Dwyer-Joyce, “Initiation of sub-surface micro-cracks and white etching areas from debonding at non-metallic inclusions in wind turbine gearbox bearing,” Wear, vol. 406–407, no. January, pp. 22–32, 2018.

[14] V. Šmeļova, A. Schwedt, L. Wang, W. Holweger, and J. Mayer, “Microstructural changes in White Etching Cracks (WECs) and their relationship with those in Dark Etching Region (DER) and White Etching Bands (WEBs) due to Rolling Contact Fatigue (RCF),” Int. J. Fatigue, vol. 100, pp. 148–158, Jul. 2017.

[15] M. H. Evans, A. D. Richardson, L. Wang, and R. J. K. Wood, “Serial sectioning investigation of butterfly and white etching crack (WEC) formation in wind turbine gearbox bearings,” Wear, vol. 302, no. 1–2, pp. 1573–1582, Apr. 2013.

[16] C. F. Kusche, J. S. K. L. Gibson, M. A. Wollenweber, and S. Korte-Kerzel, “On the mechanical properties and deformation mechanisms of manganese sulphide inclusions,” Mater. Des., vol. 193, p. 108801, Aug. 2020, doi: 10.1016/J.MATDES.2020.108801.

[17] W. Solano-Alvarez and H. K. D. H. Bhadeshia, “Distinguishing cause and effect in bearing steel failure: part 2,” Metall. Mater. Trans. A, vol. 45, p. DOI:10.1007/s11661-014-2431-x, 2014.

[18] M. H. Evans, L. Wang, H. Jones, and R. J. K. Wood, “White etching crack (WEC) investigation by serial sectioning, focused ion beam and 3-D crack modelling,” Tribol. Int., vol. 65, pp. 146–160, 2013.

[19] J. Luyckx, “White etching crack failure mode in roller bearings: From observation via analysis to understanding and an industrial solution,” ASTM Spec. Tech. Publ., vol. 1542 STP, pp. 1–25, 2012.

[20] J. F. W. Leung, R. Voothaluru, and R. W. Neu, “Predicting white etching matter formation in bearing steels using a fretting damage parameter,” Tribol. Int., vol. 159, p. 106966, Jul. 2021.

[21] M.-H. Evans, “An updated review: white etching cracks (WECs) and axial cracks in wind turbine gearbox bearings,” Mater. Sci. Technol., vol. 32, no. 11, pp. 1133–1169, Jul. 2016.

[22] A. M. Diederichs, S. Barteldes, A. Schwedt, J. Mayer, and W. Holweger, “Study of subsurface initiation mechanism for white etching crack formation,” Mater. Sci. Technol., vol. 32, no. 11, pp. 1170–1178, Jul. 2016.

[23] J. Lai and K. Stadler, “Investigation on the mechanisms of white etching crack (WEC) formation in rolling contact fatigue and identification of a root cause for bearing premature failure,” Wear, vol. 364–365, pp. 244–256, Oct. 2016.

[24] H. Yin, Y. Wu, D. Liu, P. Zhang, G. Zhang, and H. Fu, “Rolling Contact Fatigue-Related Microstructural Alterations in Bearing Steels: A Brief Review,” Met. 2022, Vol. 12, Page 910, vol. 12, no. 6, p. 910, May 2022.

[25] F. J. López-Uruñuela et al., “Broad review of ‘White Etching Crack’ failure in wind turbine gearbox bearings: Main factors and experimental investigations,” Int. J. Fatigue, vol. 145, p. 106091, Apr. 2021.

[26] R. H. Vegter and K. Stadler, “Review on Crack Initiation and Premature Failures in Bearing Applications,” ASTM Spec. Tech. Publ., vol. STP 1623, pp. 1–25, 2020.

[27] J. H. Chen, C. Xie, S. X. Li, and S. Y. Lu, “White etching area damage induced by shear localization in rolling contact fatigue of bearing steel,” Fatigue Fract. Eng. Mater. Struct., vol. 47, no. 1, pp. 170–186, Jan. 2024.

[28] B. Gould and A. Greco, “Investigating the Process of White Etching Crack Initiation in Bearing Steel,” Tribol. Lett., vol. 62, no. 2, pp. 1–14, 2016.

[29] M. Ščepanskis, A. Jakovičs, I. Kaldre, W. Holweger, B. Nacke, and A. M. Diederichs, “The Numerical Model of Electrothermal Deformations of Carbides in Bearing Steel as the Possible Cause of White Etching Cracks Initiation,” Tribol. Lett., vol. 59, no. 2, Aug. 2015.

[30] T. Plazenet and T. Boileau, “Overview of Bearing White Etching Cracks due to Electrical Currents,” 2021 IEEE 13th Int. Symp. Diagnostics Electr. Mach. Power Electron. Drives, SDEMPED 2021, pp. 440–446, 2021.

[31] B. Gould, N. Demas, R. Erck, M. C. Lorenzo-Martin, O. Ajayi, and A. Greco, “The effect of electrical current on premature failures and microstructural degradation in bearing steel,” Int. J. Fatigue, vol. 145, p. 106078, Apr. 2021.

[32] X. Z. Liang and P. E. J. Rivera-Díaz-del-Castillo, “Hydrogen-accelerated white etching area formation in bearings under rolling contact fatigue,” Int. J. Fatigue, vol. 159, p. 106753, Jun. 2022.

[33] L. Davis, P. Ramkumar, A. Panda, M. Franken, B. Vengudusamy, and J. Kondratiuk, “Microstructure alterations and white etching area formation in bearing steels under high-frequency dynamic loading,” Tribol. Int., vol. 196, p. 109676, Aug. 2024.

[34] L. Davis and P. Ramkumar, “Effect of DLC film on the mitigation of white etching areas (WEAs) under dynamic loading,” Surf. Coatings Technol., vol. 474, p. 130102, Dec. 2023.

[35] M.-H. Evans, “White structure flaking (WSF) in wind turbine gearbox bearings: effects of ‘butterflies’ and white etching cracks (WECs),” Mater. Sci. Technol., vol. 28, no. 1, pp. 3–22, Jan. 2012.

[36] W. Lacava, J. Keller, and B. McNiff, “Gearbox reliability collaborative: Test and model investigation of sun orbit and planet load share in a wind turbine gearbox,” Collect. Tech. Pap. - AIAA/ASME/ASCE/AHS/ASC Struct. Struct. Dyn. Mater. Conf., 2012.

[37] W. LaCava, Y. Xing, C. Marks, Y. Guo, and T. Moan, “Three-dimensional bearing load share behaviour in the planetary stage of a wind turbine gearbox,” IET Renew. Power Gener., vol. 7, no. 4, pp. 359–369, Jul. 2013.

[38] R. Dai & H. Long, “Predicting subsurface inclusion initiated butterfly-wing cracking under rolling contact fatigue”, International Journal of Fatigue, 188, 108533-108533, 2024.

[39] A. Ellermann and B. Scholtes, “The strength differential effect in different heat treatment conditions of the steels 42CrMoS4 and 100Cr6,” Mater. Sci. Eng. A, vol. 620, pp. 262–272, 2015.

[40] F. Ville, X. Kleber, and B. Liatard, “Understanding white etching cracks in rolling element bearings : State of art and multiple driver transposition on a twin-disc machine,” vol. 231, no. 2, pp. 203–220, 2017, doi: 10.1177/1350650116648058

[41] J. L. O’brien and A. H. King, “Electron Microscopy of Stress-Induced Structural Alterations Near Inclusions in Bearing Steels,” J. Basic Eng., vol. 88, no. 3, pp. 568–571, Sep. 1966

[42] J. A. Martin, S. F. Borgese, and A. D. Eberhardt, “Microstructural Alterations of Rolling—Bearing Steel Undergoing Cyclic Stressing,” J. Basic Eng., vol. 88, no. 3, pp. 555–565, Sep. 1966

[43] H. Harada, T. Mikami, M. Shibata, D. Sokai, A. Yamamoto, and H. Tsubakino, “Microstructural changes and crack initiation with white etching area formation under rolling/sliding contact in bearing steel,” ISIJ Int., vol. 45, no. 12, pp. 1897–1902, 2005.

[44] A. M. Diederichs, A. Schwedt, J. Mayer, and T. Dreifert, “Materials Science and Technology Electron microscopy analysis of structural changes within white etching areas Electron microscopy analysis of structural changes within white etching areas,” 2016.

[45] L. W. Liang, Y. J. Wang, Y. Chen, H. Y. Wang, and L. H. Dai, “Dislocation nucleation and evolution at the ferrite-cementite interface under cyclic loadings,” Acta Mater., vol. 186, pp. 267–277, Mar. 2020.

[46] B. Gould, A. Greco, K. Stadler, and X. Xiao, “An analysis of premature cracking associated with microstructural alterations in an AISI 52100 failed wind turbine bearing using X-ray tomography,” Mater. Des., vol. 117, pp. 417–429, Mar. 2017, doi: 10.1016/J.MATDES.2016.12.089.

Appendix A.

Table A1 Chemical composition of 100Cr6 steel material [9]

Component	C	Si	Mn	P	S	Cr	Ni	Mo	Cu
Content (wt%)	0.95-1.05	0.15-0.35	0.25-0.45	0.025 max	0.025 max	1.40-1.65	0.30 max	0.08 max	0.20 max

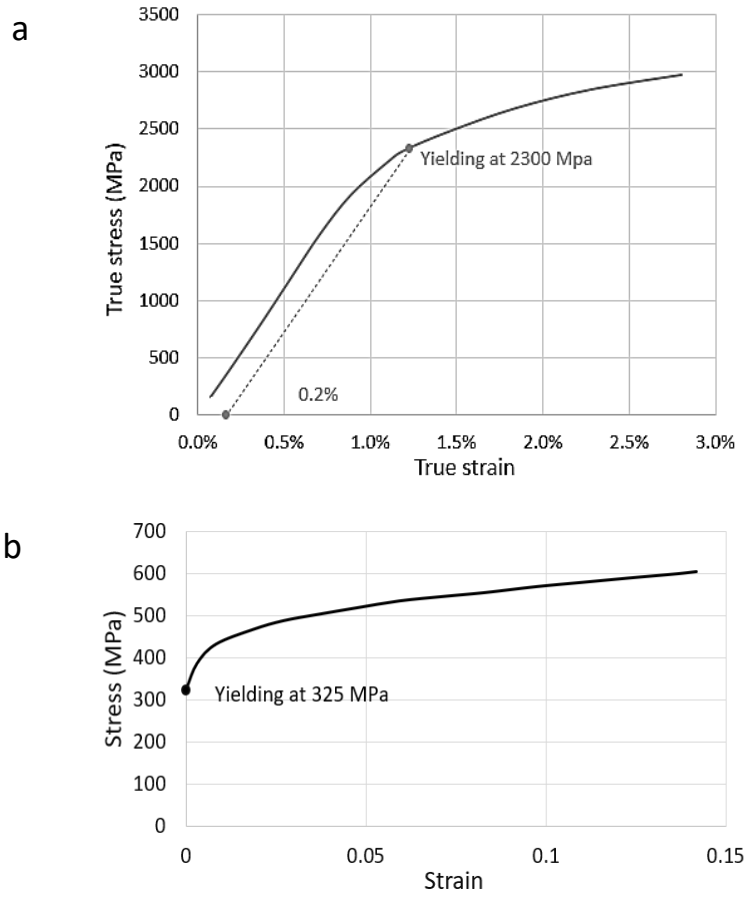

Fig. A1 Material stress-strain curves: (a) 100Cr6 steel [38]; (b) MnS inclusion [39]